© 2018. Published by The Company of Biologists Ltd | Journal of Cell Science (2018) 131, jcs203893. doi:10.1242/jcs.203893

RESEARCH ARTICLE

SPECIAL ISSUE: PLANT CELL BIOLOGY

The Golgi entry core compartment functions as a COPII-independent scaffold for ER-to-Golgi transport in plant cells

Yoko Ito[1,*], Tomohiro Uemura[2] and Akihiko Nakano[1,2]

ABSTRACT

Many questions remain about how the stacked structure of the Golgi is formed and maintained. In our previous study, we challenged this question using tobacco BY-2 cells and revealed that, upon Brefeldin A (BFA) treatment, previously undescribed small punctate structures containing a particular subset of *cis*-Golgi proteins are formed adjacent to the ER-exit sites and act as scaffolds for Golgi regeneration after BFA removal. In this study, we analyzed these structures further. The proteins that localize to these punctate structures originate from the *cis*-most cisternae. 3D time-lapse observations show that the *trans*-Golgi marker is transported through these structures during Golgi regeneration. These data indicate that the *cis*-most cisternae have a specialized region that receives cargo from the ER, which becomes obvious upon BFA treatment. Expression of a dominant mutant form of SAR1 does not affect the formation of the punctate structures. We propose to call these punctate structures the 'Golgi entry core compartment' (GECCO). They act as receivers for the rest of the Golgi materials and are formed independently of the COPII machinery.

This article has an associated First Person interview with the first author of the paper.

KEY WORDS: Golgi, BFA, SAR1, COPII, Plants

INTRODUCTION

The Golgi is an essential organelle for membrane trafficking, which functions in protein modification and sorting, and polysaccharide synthesis in plant cells in particular. Its characteristic stacked structure of disk-like cisternae is conserved among almost all eukaryotes, which makes this organelle easily distinguishable from other intracellular structures. The cisternae are polarized between the *cis*- and *trans*-sides within a stack, and glycosylation enzymes localize sequentially from *cis* to *trans* in the order in which they function (Dunphy and Rothman, 1985; Glick and Luini, 2011). Knowledge about what occurs during the biogenesis of this structure is limited to research on a few protozoans – typically organisms with only one Golgi stack per cell – yet these results have proposed a variety of schemes for Golgi generation (Benchimol et al., 2001; Bevis et al., 2002; He et al., 2004; Pelletier et al., 2002). Molecular mechanisms that govern Golgi formation remain to be unveiled.

[1]Live Cell Super-Resolution Imaging Research Team, RIKEN Center for Advanced Photonics, Wako, Saitama 351-0198, Japan. [2]Laboratory of Developmental Cell Biology, Department of Biological Sciences, Graduate School of Science, The University of Tokyo, Bunkyo-ku, Tokyo 113-0033, Japan.

*Author for correspondence (yoko.ito@riken.jp)

Y.I., 0000-0002-9877-1596; T.U., 0000-0001-7270-7986; A.N., 0000-0003-3635-548X

Received 15 March 2017; Accepted 17 August 2017

Brefeldin A (BFA), a compound that inhibits the activity of guanine nucleotide exchange factors for ARF GTPases (Chardin and McCormick, 1999), has been used as a tool to investigate Golgi assembly in mammalian cells, because its treatment leads to relocalization of Golgi proteins into the ER in a reversible manner (Alcalde et al., 1992; Puri and Linstedt, 2003). Similar disassembly and reassembly of the Golgi is also observed upon BFA treatment and removal in tobacco cells (Langhans et al., 2007; Ritzenthaler et al., 2002; Schoberer et al., 2010). Taking advantage of this, we previously performed multicolor time-lapse observation of Golgi proteins during BFA treatment and removal in tobacco BY-2 cultured cells. We found that previously unknown punctate structures, in which a particular subset of *cis*-Golgi proteins localize, are formed in the vicinity of the ER exit sites (ERES) upon BFA treatment and that they function as the scaffold for Golgi regeneration after BFA removal, which proceeds in the *cis* to *trans* direction (Ito et al., 2012). We propose to call these punctate structures GECCO (the Golgi entry core compartment) hereafter, for the reasons described herein.

Our earlier findings raised several new questions: (1) What is the difference between the *cis*-Golgi proteins that concentrate to GECCO and those that relocalize to the ER upon BFA treatment? (2) Are the Golgi components that have been relocated to the ER by BFA sent back to the original positions through GECCO after BFA removal? (3) What transport machinery is involved in the formation of GECCO? In this report, we address these questions by using powerful live-imaging techniques.

RESULTS

SYP31 and RER1B localize to the *cis*-most region of the Golgi stacks

In our previous work, we found that *cis*-Golgi proteins SYP31 and RER1B localize to GECCO upon BFA treatment, whereas another *cis*-Golgi marker ERD2 changes its localization to the ER completely (Ito et al., 2012). In order to determine what is different between these two types of *cis*-Golgi proteins, we observed their intra-Golgi localization in detail by establishing a BY-2 cell line expressing two *cis*-Golgi proteins and a *trans*-Golgi protein (ST) labeled with three different colors simultaneously. As shown in Fig. 1A,B, localization of GFP–SYP31 and ERD2–YFP in comparison to the *trans* marker ST–mRFP were slightly different. GFP–SYP31 localized to the extreme *cis* side in the Golgi stacks. GFP–RER1B and mRFP–SYP31 showed mostly overlapping localization that was distinct from ST–YFP (Fig. 1C,D). Although the intra-Golgi localization of ERD2 was relatively broad, its fluorescence peak was subtly different from that of the medial-Golgi marker XYLT (β1,2-xylosyltransferase; Pagny et al., 2003; Fig. S1A,B). This means that the ERD2 signal mainly represents cisternae distinct from the medial-Golgi. In addition, mRFP–SYP31 showed a different intra-Golgi localization to that of ManI (α-1,2-mannosidase I; Fig. S1C,D), which relocated to the ER upon BFA treatment (Fig. S1E). Because ManI functions as the first *N*-glycosylation enzyme in the Golgi, it was thought to

Journal of Cell Science (2018) 131, jcs203893. doi:10.1242/jcs.203893

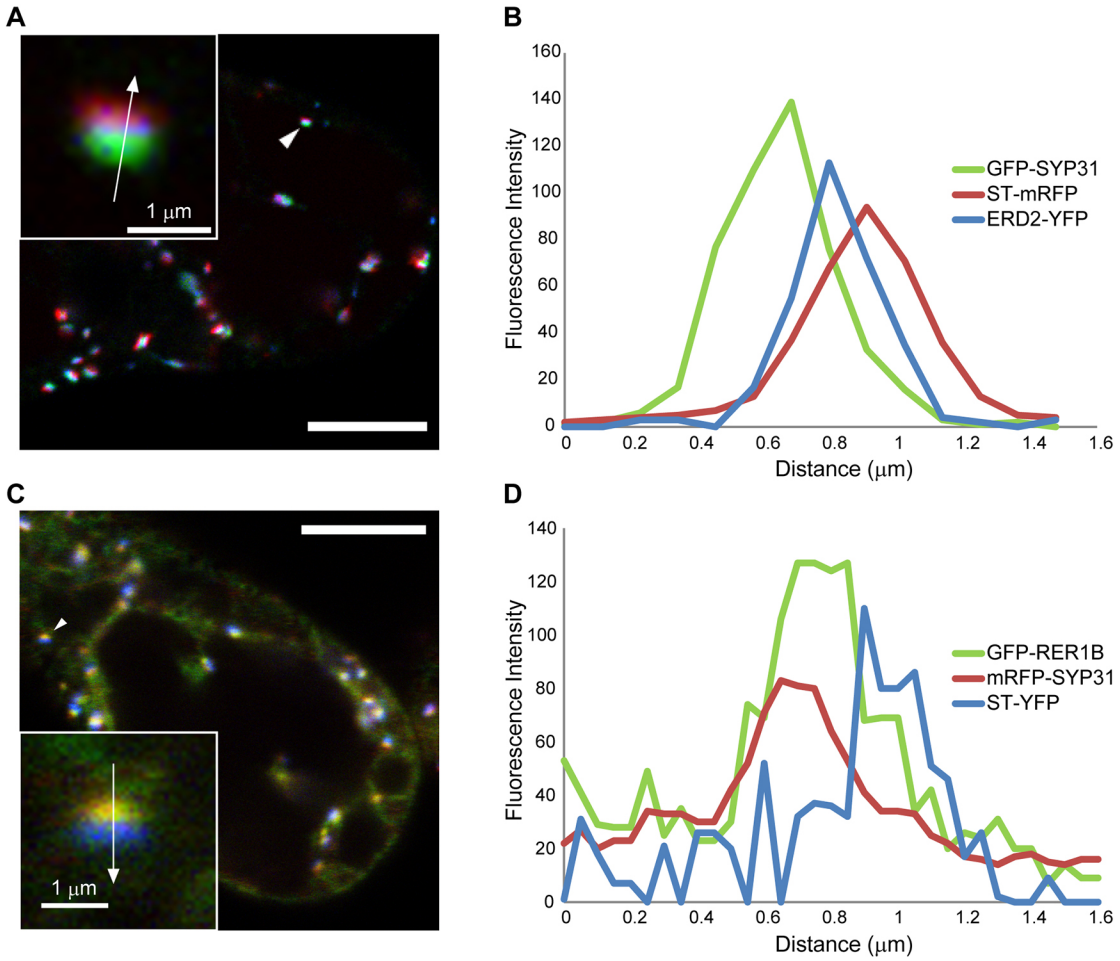

Fig. 1. Detailed intra-Golgi localization of Golgi markers. (A) Confocal triple-colored observation of BY-2 cells expressing GFP–SYP31 (green), ST–mRFP (red) and ERD2–YFP (blue). The stack magnified in the inset is indicated by an arrowhead. (B) The fluorescent profile along the arrow in the inset of A. (C) Confocal triple-colored observation of BY-2 cells expressing GFP-RER1B (green), mRFP-SYP31 (red), and ST-YFP (blue). The stack magnified in the inset is indicated by an arrowhead. (D) The fluorescent profile along the arrow in the inset of C. Representative images from at least five independent cells for each cell line. Scale bars: 10 μm (insets, 1 μm).

localize at the *cis*-most side of the stacks. However, an immunolocalization analysis revealed that it localizes at the third to fourth cisternae, not at the first and second *cis* cisternae (Donohoe et al., 2013). Our observations indicate that SYP31 and RER1B, the *cis*-Golgi markers that localize to GECCO upon BFA treatment, originally reside in the *cis*-most region of the Golgi, presumably at the first to second cisternae.

ST–mRFP is transported through GECCO during Golgi regeneration

As we reported previously, regeneration of the Golgi stacks after removal of BFA begins by coalescence of GECCO with GFP–SYP31 signals, and ST–mRFP is gradually concentrated next to the regenerating *cis*-cisternae. However, it was unclear whether ST–mRFP was transported via GECCO (Ito et al., 2012).

To examine the role of GECCO in transport of other Golgi proteins during Golgi regeneration, we observed the Golgi and the ER markers using super-resolution confocal live-imaging microscopy (SCLIM; Kurokawa et al., 2013). SCLIM enables live-cell 3D time-lapse (4D) imaging with extremely high speed and high resolution in multiple colors at the same time, and thus provides us with information that was not previously available. In order to visualize the *cis*- and *trans*-Golgi and the ER simultaneously, we used near-infrared fluorescent protein (iRFP) as the third fluorescent protein (Filonov et al., 2011). We constructed a derivative of the fluorescent ER marker SP–iRFP-HDEL, iRFP fused with the signal peptide (SP) from *Arabidopsis* endo-xyloglucan transferase and the HDEL ER retrieval signal (Takeuchi et al., 2000), and introduced it into a BY-2 cell line already expressing GFP–SYP31 and ST–mRFP. By adding biliverdin (the chromophore of iRFP) to the culture, we could observe the tubular network unique to the ER with Golgi stacks in 3D (Fig. 2). Using this cell line, we observed Golgi regeneration after BFA removal. In order to inhibit the *de novo* synthesis of marker proteins and to halt the movement of organelles by depolymerizing actin fibers, cycloheximide and latrunculin B (LatB) were added to the culture. ST-mRFP transiently colocalized with GFP–SYP31 at GECCO (Fig. 3A, 2:55–3:55), and then the two fluorescent signals were segregated into *cis* and *trans* localizations (Fig. 3A, 5:00–5:35). The 3D images of ST–mRFP and GFP–SYP31 colocalization at GECCO showed a mosaic distribution (Fig. 3B). Pearson's correlation coefficients in 3D between GFP–SYP31 and ST–mRFP exhibited an increase over time and a subsequent decrease to the initial level, whereas that between ST-mRFP and SP-iRFP-HDEL decreased continuously (Fig. 3C, Fig. S2A,B). Such an increase of the correlation between SYP31 and ST was not observed either in the cells without BFA (Fig. 3D) or in cells with continued BFA treatment

Journal of Cell Science (2018) 131, jcs203893. doi:10.1242/jcs.203893

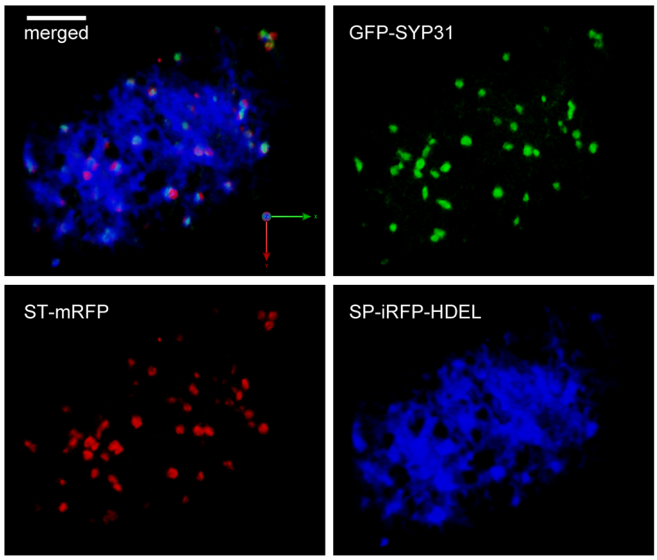

Fig. 2. 3D visualization of the ER using iRFP. 3D images of a BY-2 cell expressing GFP–SYP31 (*cis*, green), ST–mRFP (*trans*, red) and SP–iRFP-HDEL (ER, blue). The cell was observed by SCLIM with optical slices 0.1 µm apart along the *z*-axis. 3D images were reconstructed and deconvolved to obtain a higher resolution. Biliverdin was added to the culture 4 h before observation. Representative image from at least 10 independent cells. Scale bar: 5 µm.

(Fig. S2C). These data suggest that ST–mRFP that has exited the ER after BFA removal is first transported to GECCO where GFP–SYP31 resides, and then localizes to the regenerated *trans*-cisternae.

Transport of SYP31 to GECCO is not inhibited by BFA or a dominant SAR1 mutant

Only a subset of *cis*-Golgi proteins behave differently from other Golgi proteins and are localized to GECCO upon BFA treatment. We examined whether newly synthesized SYP31 is transported from the ER to GECCO in the presence of BFA. As a control, we transformed BY-2 cells with dexamethasone (DEX)-inducible mRFP-tagged SYP22 (also known as VAM3, a vacuolar membrane SNARE). When DEX and BFA were added to the cell culture at the same time, newly synthesized mRFP–SYP22 did not reach the vacuole but localized to the ER membrane, colocalizing with the ER marker SP–GFP-HDEL (Fig. 4A). This indicates that the ER exit of mRFP–SYP22 was inhibited by BFA treatment. Likewise, when the DEX-inducible mRFP–SYP31 cell line was treated with DEX and BFA simultaneously, mRFP–SYP31 localized to GECCO, similar to the results observed when BFA was added after mRFP–SYP31 induction (Fig. 4B). This indicates that transport of SYP31 from the ER to GECCO was not inhibited by BFA.

Next, we examined whether the COPII machinery is involved in the transport of SYP31 to GECCO. The COPII coat plays a central role in ER-to-Golgi transport, and its assembly is regulated by SAR1 GTPase (Brandizzi and Barlowe, 2013; Sato and Nakano, 2007). Expression of the GTP-fixed mutant form of SAR1 GTPase (SAR1 H74L) is known to have a dominant-negative effect on ER–Golgi transport (Osterrieder et al., 2009; Takeuchi et al., 1998, 2000). We introduced DEX-inducible NtSAR1 H74L into the cell line stably expressing GFP–SYP31 and ST–mRFP. As shown in Fig. 5A, the induction of NtSAR1 H74L led to the localization of ST-mRFP to the ER and of GFP–SYP31 to GECCO, similar to results with BFA treatment. The fluorescence profile around GECCO was markedly different from that in the control Golgi. ST–mRFP on the ER did not show apparent accumulation near GECCO (compare Fig. S3A,B), indicating that ST–mRFP is almost evenly dispersed on the ER. In order to examine ER-to-GECCO transport, we established a cell line in which GFP–SYP31 and ST–mRFP can be concurrently induced by estradiol treatment (Fig. 5B), and further transformed it with DEX-inducible NtSAR1 H74L. After 24 h of DEX treatment, the same condition that caused relocalization of stably expressed ST–mRFP, we added estradiol to induce the Golgi markers. The newly expressed ST–mRFP localized to the ER, and GFP–SYP31 showed GECCO localization (Fig. 5C). The fluorescent profile showed no obvious accumulation of ST–mRFP near GECCO (Fig. 3C). These data indicate that the localization of SYP31 to GECCO does not depend on the COPII machinery.

DISCUSSION

The *cis*-most cisternae of plant Golgi stacks have an ERGIC-like nature

In this study, we found that the proteins that localize to what we propose to call GECCO upon treatment with BFA, are normally localized to the *cis*-most region of the Golgi stack (Fig. 6A,B). These observations suggest that the *cis*-most cisternae have a different property from the rest of the Golgi cisternae in plant cells.

In vertebrate cells, in which Golgi stacks are concentrated near the nucleus to form a large ribbon-like structure, the Golgi is far from the ERES (Wei and Seemann, 2010). In order to carry out this long-distance transport, the ER-Golgi intermediate compartment (ERGIC) functions as a cargo-sorting station between the ER and the Golgi (Appenzeller-Herzog and Hauri, 2006). By contrast, in plant cells, the Golgi stacks and the ERES are always closely associated and therefore ERGIC was believed to be nonexistent in plants. In our previous report, however, we noticed the similarity between the punctate *cis*-Golgi compartment formed upon BFA treatment (which we now call GECCO) in plant cells and the ERGIC in vertebrate cells, because they both act as the scaffold for Golgi formation/regeneration (Ito et al., 2012). We speculated that this special *cis*-Golgi compartment quickly matures or merges into *cis*-cisternae under normal conditions and is exaggerated and becomes visible when their maturation is arrested by BFA.

Now, taking the new data into consideration, we would like to update our model. An ERGIC marker ERGIC-53 is known to localize to punctate structures near the ERES upon BFA treatment in mammalian cells, which are called ‘Golgi remnants’ (Lippincott-Schwartz et al., 1990). GECCO, the punctate structure of *cis*-Golgi markers formed adjacent to the ERES upon BFA treatment in plant cells, is more like these Golgi remnants of mammalian cells. SYP31 and RER1B, which localize to GECCO in the presence of BFA, normally localize to the *cis*-most region of the Golgi. We propose that the *cis*-most cisternae in plant cells originally have a property corresponding to the ERGIC, and harbor a functional domain to receive cargo from the ER (GECCO). An immuno-electron microscopy study has also suggested that the *cis*-most cisternae in plant cells are biosynthetically inactive and function as sorting compartments, similar to ERGIC (Donohoe et al., 2013). Plants and vertebrates share the fundamental machinery at the ER-Golgi interface, albeit with different spatial arrangements.

GECCO receives other Golgi components during Golgi regeneration

Because our previous study provided evidence for the role of GECCO as the scaffold for Golgi reassembly, we now aimed to observe the transport processes at this scaffold in 3D in detail. The high-speed and high-sensitivity SCLIM, a super-resolution live-imaging microscopy

Journal of Cell Science (2018) 131, jcs203893. doi:10.1242/jcs.203893

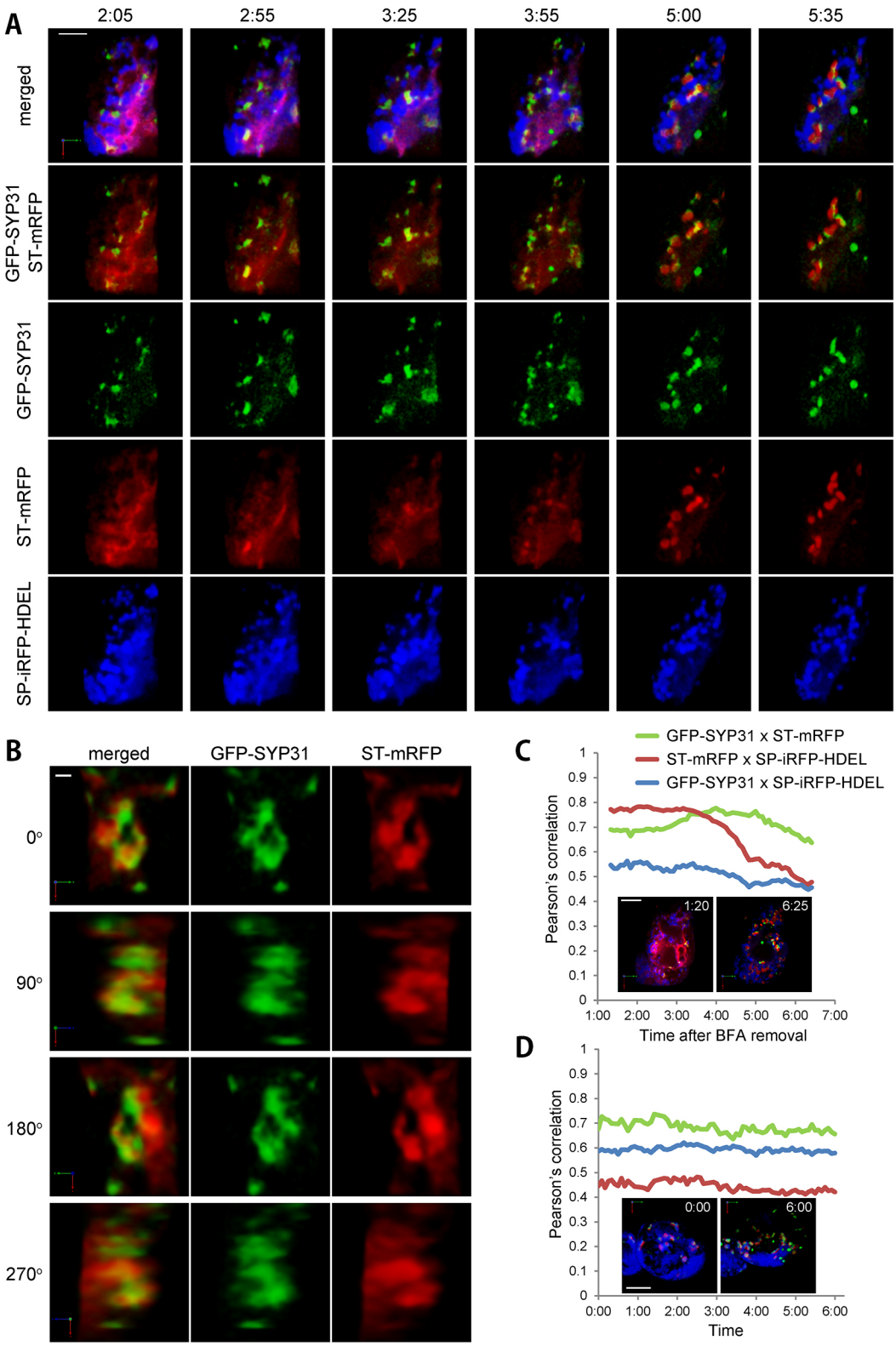

Fig. 3. Regeneration of the Golgi after removal of BFA observed in 3D. (A) 3D time-lapse images of BY-2 cells expressing GFP–SYP31 (*cis*, green), ST–mRFP (*trans*, red) and SP–iRFP-HDEL (ER, blue) after BFA removal. The cells were treated with BFA for 2 h, and then BFA was washed out. LatB was added 30 min before removal of BFA, and cycloheximide and biliverdin were added at the point of BFA removal. Observations started 1 h 20 min after BFA removal using SCLIM with optical slices 0.2 µm apart along the *z*-axis. 3D image sets captured at 5 min intervals were reconstructed and deconvolved. Indicated times are the elapsed time after BFA removal (h:min). (B) Magnified 3D SCLIM images of the cell shown in A, 3 h 20 min after BFA removal. GFP–SYP31 (*cis*, green) and ST–mRFP (*trans*, red). The images rotated by 90° steps around *y*-axis are presented. (C) Change of 3D Pearson's correlation coefficients of the Golgi and ER markers over time in the cell shown in A. The indicated times are the elapsed time after BFA removal. (D) Change of 3D Pearson's correlation coefficients in cells without BFA treatment. LatB, cycloheximide and biliverdin were added to the culture at 1 h 30 min before the start of observation. Scale bars: 5 µm (A), 1 µm (B), 10 µm (C,D).

Journal of Cell Science (2018) 131, jcs203893. doi:10.1242/jcs.203893

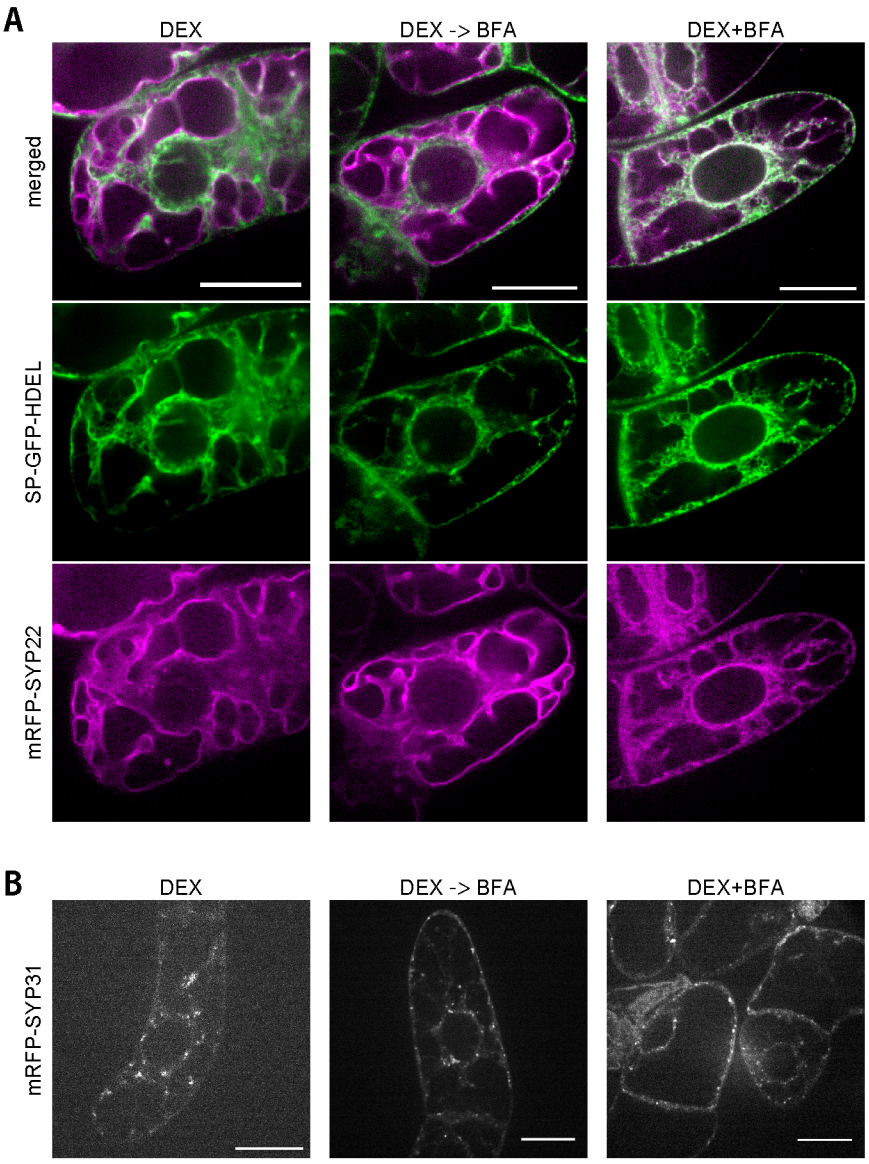

Fig. 4. Induction of fluorescent markers combined with BFA treatment. (A) Confocal images of BY-2 cells with stably expressed SP–GFP-HDEL (green) and DEX-inducible mRFP–SYP22 (magenta). After 6 h of DEX treatment (left), after 6 h of DEX treatment followed by BFA treatment for an additional 2 h (middle) and 6 h after addition of DEX and BFA at the same time (right). (B) Confocal images of BY-2 cells with DEX-inducible mRFP–SYP31. After 4 h of DEX treatment (left), after 4 h of DEX treatment followed by BFA treatment for an additional 2 h (middle) and 4 h after addition of DEX and BFA at the same time (right). Representative images from at least five independent cells for each condition. Scale bars: 20 µm.

we have developed (Kurokawa et al., 2013), now enables us to make 4D observations with triple colors at low laser powers, which avoids the photodamage that can halt Golgi regeneration.

In the 4D data, we see temporary colocalization of ST–mRFP with GFP–SYP31 at GECCO during regeneration. Correlation coefficients between these markers increase during this step, and then decrease as typical side-by-side localization of *cis*- and *trans*-Golgi appears. The temporal increase of colocalization is small in extent but is significant and reproducible (see Figs 2 and 3). These results indicate that ST–mRFP is initially transported to GECCO, rather than directly localizing to the reassembling *trans*-cisternae (Fig. 6C,D).

During the colocalization, GFP–SYP31 and ST–mRFP are not mixed evenly and show mosaic patterns. This is quite similar to the distribution patterns of earlier and later Golgi markers coexisting within one maturing cisterna in *Saccharomyces cerevisiae* (Ishii et al., 2016; Matsuura-Tokita et al., 2006). Although the mechanism of this domain formation is yet to be investigated, it is reasonable that such segregation of different Golgi proteins contributes to their efficient sorting and transport. The similar segregation of *cis*- and *trans*-Golgi markers at GECCO after removal of BFA presumably indicates that the Golgi stacks regenerate by using the mechanism of cisternal maturation.

COPII-independent Golgi entry core compartment (GECCO) as the first platform for ER-Golgi transport

COPII is the central mechanism of the ER-to-Golgi anterograde transport, and its disruption by dominant-mutant forms of SAR1 is well known to arrest ER exit of many kinds of cargo in yeast (Nakano et al., 1994), mammals (Kuge et al., 1994) and plants (reviewed in Ito et al., 2014). Indeed, in the present study, we have shown that the ER exit of ST–mRFP is blocked by the SAR1 H74L mutant. In mammalian cells, ERGIC-53 is trapped in the ER by dominant-negative SAR1 (Hauri et al., 2000; Shima et al., 1998). However, in tobacco leaf epidermal cells, *cis*-Golgi matrix proteins are reported to localize not only to the ER but also to small punctate structures upon expression of NtSAR1 H74L, depending on the cells and transformation methods used (Osterrieder et al., 2009). The authors suggested that this variation of localization is due to the difference in expression timing between the fluorescent Golgi proteins and NtSAR1 H74L; the Golgi proteins that had already been exported from the ER before blockage by NtSAR1 H74L were

Journal of Cell Science (2018) 131, jcs203893. doi:10.1242/jcs.203893

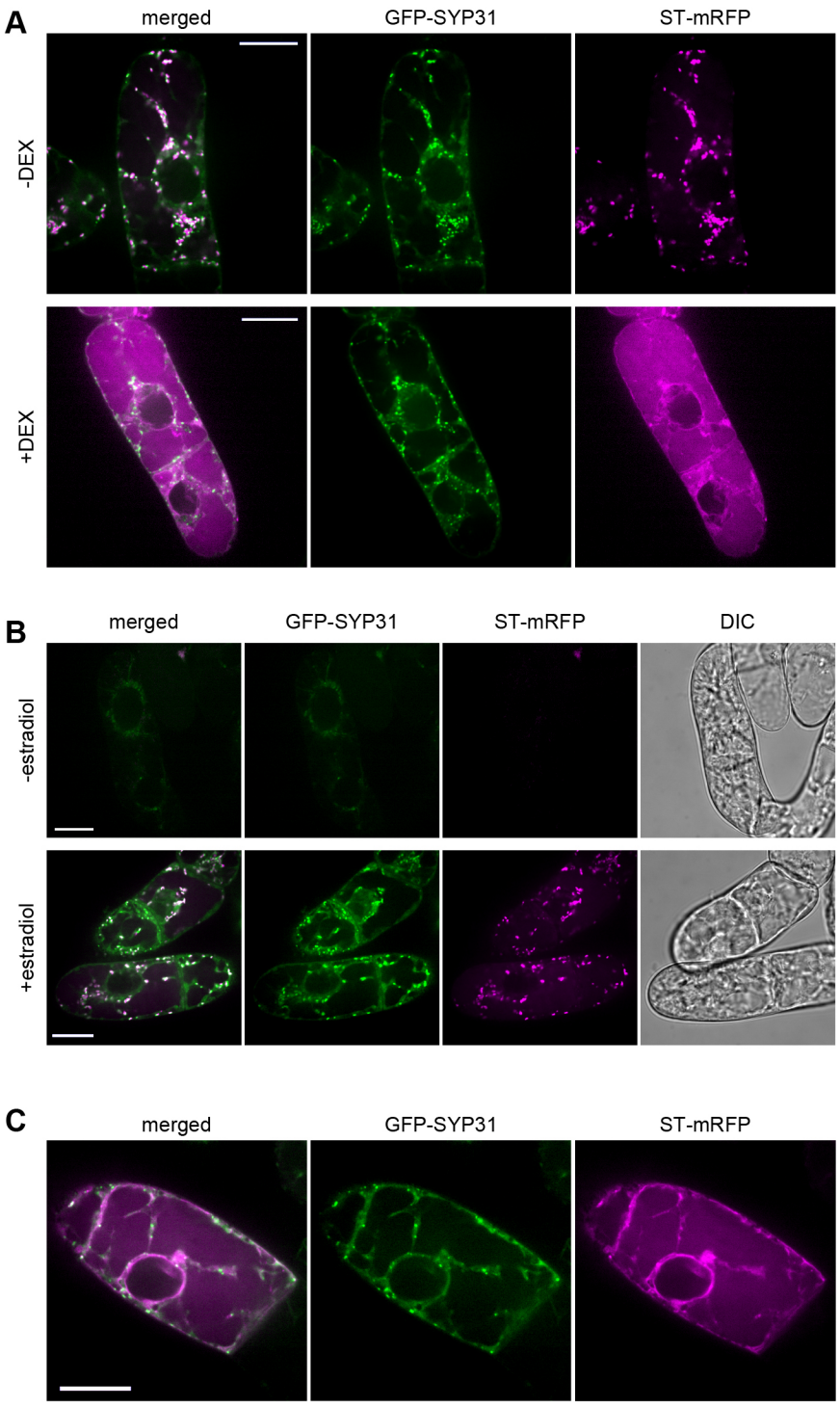

Fig. 5. Effects of NtSAR1 H74L induction upon stably or inducibly expressed Golgi markers. Confocal images of BY-2 cells with GFP–SYP31 (*cis*, green) and ST–mRFP (*trans*, magenta). (A) The cells with stably expressed GFP–SYP31, ST–mRFP and DEX-inducible NtSAR1 H74L. Without induction (−DEX) and after induction with 24 h of DEX treatment (+DEX). (B) The cells with estradiol-inducible GFP–SYP31 and ST–mRFP. Without induction (−estradiol) and with induction by 24 h of estradiol treatment (+estradiol). (C) The cells with time-shift induction of NtSAR1 H74L and GFP–SYP31/ST-mRFP. NtSAR1 H74L was induced by 24 of DEX treatment in advance, and estradiol was added subsequently to induce GFP–SYP31 and ST–mRFP. Observation was performed 24 h after estradiol addition. Representative images from at least seven independent cells for each condition. Scale bars: 20 µm.

left at the punctate structures after ER-exit arrest. In our present study, we do not observe any cells with GFP–SYP31 solely localizing to the ER upon induction of NtSAR1 H74L. SYP31 is still transported to GECCO when NtSAR1 H74L is induced sufficiently earlier than Golgi markers by time-shift dual induction. Therefore, we propose that a 'core' compartment for Golgi entry (GECCO) exists with a particular set of Golgi proteins (components of the *cis*-most cisternae) in plant cells, the formation of which is independent of the COPII mechanism (Fig. 6B). Although COPII-independent events in the ER-to-Golgi traffic are not well understood and may be provocative, our findings provide a good opportunity to consider whether this is a plant-specific phenomenon or could be applicable to other organisms such as mammals and yeast. Obviously, more extensive analysis on proteins trafficking across ER–GECCO–ERGIC–Golgi will be necessary to bring us further insights.

As described above, we defined the compartment where a particular set of *cis*-Golgi proteins accumulate upon BFA treatment as the Golgi entry core compartment (GECCO). We would like to further extend this definition. GECCO can exist under normal conditions, maybe quickly maturing or merging into the *cis*-most cisternae, and receive COPII vesicles at the ER–Golgi interface. In

Journal of Cell Science (2018) 131, jcs203893. doi:10.1242/jcs.203893

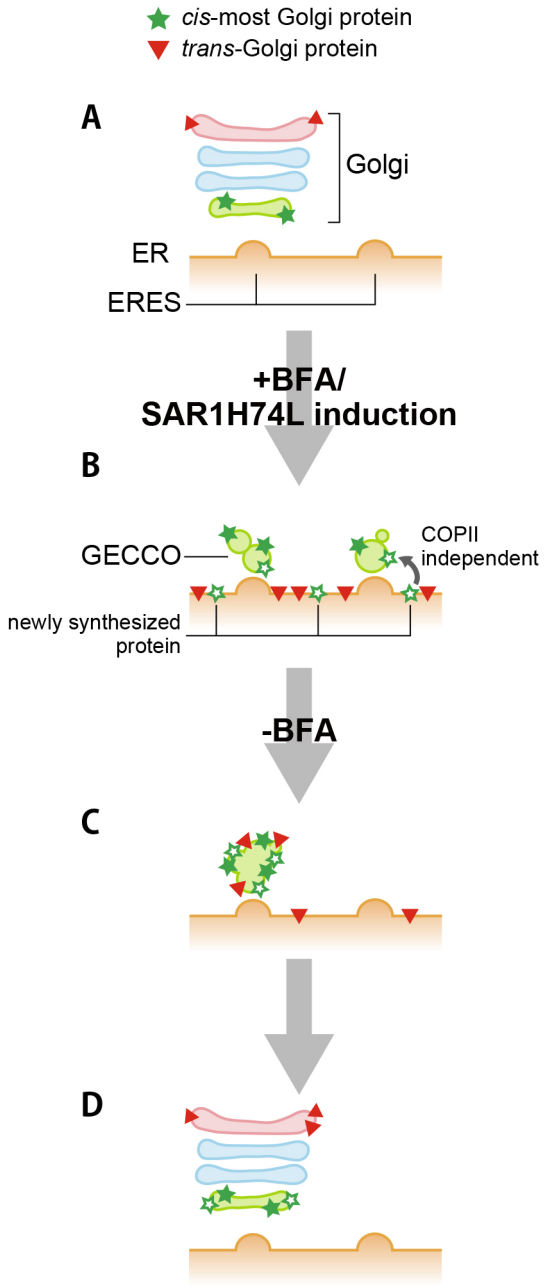

Fig. 6. A model for the behavior of the Golgi upon BFA treatment or SAR1H74L induction and BFA removal. (A) The Golgi stacks are located near the ERES. (B) By BFA treatment or SARH74L induction, proteins originate from the *cis*-most cisternae localize to GECCO and *trans*-Golgi proteins relocate to the ER membrane. Newly synthesized *cis*-most proteins can be transported from the ER to GECCO under this condition. (C) After BFA removal, *trans*-Golgi proteins exit the ER and travel through GECCO. (D) The Golgi stacks reassemble from GECCO.

other words, its important role is to function as the entry compartment of the Golgi generation, existing as a functional domain in the *cis*-most cisternae.

In *S. cerevisiae*, observations by SCLIM have revealed that ER-to-Golgi transport is mediated by the hug-and-kiss action of the *cis*-Golgi; it approaches and contacts the ERES to receive cargo (Kurokawa et al., 2014; Robinson et al., 2015). If this mechanism also operates during formation of new *cis* cisternae, some special compartment needs to pre-exist in front of the ER to receive components to build *cis*-Golgi. In the classical cisternal maturation model, the *cis*-most cisterna is assumed to form by coalescence of ER-derived COPII vesicles and perhaps COPI vesicles (Glick and Luini, 2011; Nakano and Luini, 2010); however, this is not consistent with the pre-existence of the receiver compartment that fulfills the hug-and-kiss action. We suggest that a special *cis*-Golgi compartment in yeast plays a role as GECCO and contributes as the receiver for the hug-and-kiss transport. Whether it is formed independently of COPII is a very interesting question that should be addressed.

COPII is the only mechanism known to date at the molecular level to be responsible for the ER-to-Golgi anterograde trafficking. Although there are several reports arguing for COPII-independent cargo transport from the ER in yeast, *Drosophila* and mammalian cells, such systems appear to bypass the Golgi after the exit from the ER (Grieve and Rabouille, 2011; Rabouille, 2017). A study on mammalian cells reported that transport of procollagen-I was inhibited by silencing of Sar1 but that of VSV-G and albumin was not (Cutrona et al., 2013). Under these conditions, the typical spatial organization of the ER–Golgi boundary was impaired, but mini Golgi stacks were observed in the vicinity of the ER. The authors suggested that COPI played a role in bypassing COPII (Cutrona et al., 2013). In our present study, as SYP31 exits the ER and localizes to GECCO in the presence of BFA, the involvement of the COPI machinery is unlikely in this COPII-independent pathway. Elucidation of the molecular mechanisms of this novel traffic route and the formation of GECCO would impact our understanding about Golgi generation.

MATERIALS AND METHODS

Construction of plasmids

To generate *ERD2-YFP*, *ST-YFP*, and *ManI-YFP* constructs, DNA fragments coding for *ERD2*, *ST* and *ManI* were amplified by PCR and cloned into pENTR/D-TOPO (Thermo Fisher Scientific/Invitrogen, Waltham, MA), and recombined into pK7YWG2 (Karimi et al., 2005) by LR Clonase II (Thermo Fisher Scientific/Invitrogen). *ERD2-mRFP* construct was generated by recombining *ERD2* in pENTR/D-TOPO into pH7RWG2 (Karimi et al., 2005). For *SP-iRFP-HDEL*, the *GFP* region of *SP-GFP-HDEL* (Takeuchi et al., 2000) was replaced by the DNA fragment coding for *iRFP* by In-Fusion HD Cloning Kit (Takara Bio/Clontech, Shiga, Japan). *XYLT-GFP* is a kind gift from Keiko Shoda (RIKEN, Japan).

For the DEX-inducible constructs, we modified pTA7002 (Aoyama and Chua, 1997). The T-DNA region (from RB to LB) of pKGW (Karimi et al., 2002) was replaced with the T-DNA region of pTA7002, and the sequence encoding the *hpt* gene in the T-DNA region of this vector was replaced with the *nptII* gene by In-Fusion. Next, the DNA fragment of the attR1–attR2 region of pHGW (Karimi et al., 2002) was inserted into the *Xho*I site. The resulting plasmid was designated pTASKGW (made from pTA7002, Spe^{r} in bacteria and Km^{r} in plants, with a Gateway cassette). To generate DEX-inducible fluorescent markers, the DNA fragments coding for *mRFP-SYP22* and *mRFP-SYP31* were amplified by PCR and cloned into pENTR/D-TOPO, followed by recombination into pTASKGW by LR Clonase II. For the construction of DEX-inducible *NtSAR1 H74L*, the DNA fragment encoding *NtSAR1* (GenBank accession number: D87821) was amplified from BY-2 cDNA by PCR, and cloned into pENTR/D-TOPO. To introduce a mutation, the whole vector was amplified by PCR using a mutagenesis primer set (5′-GGAGGTCTTCAGATCGCTCGCCGTGTC-3′ and 5′-GATCTGAAGACCTCCTAAATCAAACGCTTTGAA-3′) by PrimeSTAR Max DNA Polymerase (Takara Bio), and directly transformed into *E. coli* to obtain a self-circularized plasmid with *NtSAR1 H74L*. This was subcloned into pTASKGW by LR Clonase II.

To generate estradiol-inducible *GFP-SYP31/ST-mRFP*, DNA fragments coding for *GFP-SYP31* and *ST-mRFP* were first cloned into pMDC7 (Curtis and Grossniklaus, 2003). The DNA region from O_{lexA}*-46* to T_{3A} of pMDC7 harboring *GFP-SYP31* was amplified by PCR, and inserted into the *Kpn*I site of pMDC7 harboring *ST-mRFP*.

Establishment of transgenic BY-2 cell lines

Maintenance of tobacco (*Nicotiana tabacum*) bright yellow-2 (BY-2) culture is described in Nagata et al. (1992). Transformation procedures are described in Ito et al. (2012).

Drug treatments

BFA (50 µM) treatment and removal, and LatB (2 µM) and cycloheximide (100 µM) treatments are described in Ito et al. (2012). For gene induction, 10 mM stock solution of dexamethasone (Wako, Tokyo, Japan) diluted in DMSO was added to suspension cultures at 10 µM in the final concentration. Similarly, 20 mM stock solution of β-estradiol (Sigma-Aldrich, St Louis, MO) diluted in DMSO was used at 20 µM final concentration. For fluorescence observation of iRFP, biliverdin hydrochloride (Frontier Scientific, Logan, UT) diluted in DMSO at 25 mM was used at 25 µM in the final concentration. The timings when these drugs were added are indicated in figure legends.

Confocal microscopy

2D triple-colored observations and double-colored observations for Fig. 1 were made under a confocal laser-scanning microscope (model LSM780; Zeiss, Jena, Germany). 2D single- and double-colored observations except for Fig. 1 were also done under a BX52 microscope (Olympus, Tokyo, Japan) equipped with a confocal scanner unit (model CSU10; Yokogawa Electric, Tokyo, Japan) and a cooled digital CCD camera (model ORCA-ER; Hamamatsu Photonics, Shizuoka, Japan). 3D imaging was performed by the SCLIM system we developed (Kurokawa et al., 2013), consisting of the Olympus model IX-71 fluorescence microscope with a custom-made high-speed confocal scanner (Yokogawa Electric), image intensifiers (Hamamatsu Photonics) with a custom-made cooling system, and EM-CCD cameras (Hamamatsu Photonics). The objective lens was oscillated vertically by a custom-made piezo actuator system (Yokogawa Electric). The cells were placed on 35 mm glass-bottom dishes with poly-L-lysine coating (Matsunami, Osaka, Japan), and incubated on a thermos-controlled stage (Tokai Hit, Shizuoka, Japan) maintained at 28°C. Data were subjected to deconvolution analysis with Volocity (Perkin Elmer, Waltham, MA) using the theoretical point-spread function for the spinning-disk confocal system. Images were processed and analyzed with ImageJ 1.49i (National Institutes of Health, Bethesda, MD), Photoshop CS6 (Adobe System, San Jose, CA), and Volocity.

Acknowledgements

We thank T. Nakagawa (Shimane University, Japan), N.-H. Chua (Rockefeller University, USA) and K. Shoda (RIKEN, Japan) for sharing materials.

Competing interests

The authors declare no competing or financial interests.

Author contributions

Conceptualization: Y.I., T.U., A.N.; Methodology: Y.I., T.U.; Validation: Y.I.; Formal analysis: Y.I.; Investigation: Y.I.; Writing - original draft: Y.I.; Writing - review & editing: T.U., A.N.; Visualization: Y.I.; Supervision: T.U., A.N.; Funding acquisition: Y.I., A.N.

Funding

This work was supported by a Grant-in-Aid for Scientific Research (S) to A.N. (grant number 25221103) and Grant-in-Aid for Research Activity Start-up to Y.I. (grant number 26891028) from Japan Society for the Promotion of Science, and also by the 4D measurements for Multilayered Cellular Dynamics Projects of RIKEN to A.N.

Supplementary information

Supplementary information available online at
http://jcs.biologists.org/lookup/doi/10.1242/jcs.203893.supplemental

References

Alcalde, J., Bonay, P., Roa, A., Vilaro, S. and Sandoval, I. V. (1992). Assembly and disassembly of the Golgi complex: two processes arranged in a *cis-trans* direction. *J. Cell Biol.* **116**, 69-83.

Aoyama, T. and Chua, N.-H. (1997). A glucocorticoid-mediated transcriptional induction system in transgenic plants. *Plant J.* **11**, 605-612.

Appenzeller-Herzog, C. and Hauri, H.-P. (2006). The ER-Golgi intermediate compartment (ERGIC): in search of its identity and function. *J. Cell Sci.* **119**, 2173-2183.

Benchimol, M., Consort Ribeiro, K., Meyer Mariante, R. and Alderete, J. F. (2001). Structure and division of the Golgi complex in *Trichomonas vaginalis* and *Tritrichomonas foetus*. *Eur. J. Cell Biol.* **80**, 593-607.

Bevis, B. J., Hammond, A. T., Reinke, C. A. and Glick, B. S. (2002). *De novo* formation of transitional ER sites and Golgi structures in *Pichia pastoris*. *Nat. Cell Biol.* **4**, 750-756.

Brandizzi, F. and Barlowe, C. (2013). Organization of the ER-Golgi interface for membrane traffic control. *Nat. Rev. Mol. Cell Biol.* **14**, 382-392.

Chardin, P. and McCormick, F. (1999). Brefeldin A: the advantage of being uncompetitive. *Cell* **97**, 153-155.

Curtis, M. D. and Grossniklaus, U. (2003). A gateway cloning vector set for high-throughput functional analysis of genes in planta. *Plant Physiol.* **133**, 462-469.

Cutrona, M. B., Beznoussenko, G. V., Fusella, A., Martella, O., Moral, P. and Mironov, A. A. (2013). Silencing of mammalian Sar1 isoforms reveals COPII-independent protein sorting and transport. *Traffic* **14**, 691-708.

Donohoe, B. S., Kang, B.-H., Gerl, M. J., Gergely, Z. R., McMichael, C. M., Bednarek, S. Y. and Staehelin, L. A. (2013). *Cis*-Golgi cisternal assembly and biosynthetic activation occur sequentially in plants and algae. *Traffic* **14**, 551-567.

Dunphy, W. G. and Rothman, J. E. (1985). Compartmental organization of the Golgi stack. *Cell* **42**, 13-21.

Filonov, G. S., Piatkevich, K. D., Ting, L.-M., Zhang, J., Kim, K. and Verkhusha, V. V. (2011). Bright and stable near-infrared fluorescent protein for in vivo imaging. *Nat. Biotechnol.* **29**, 757-761.

Glick, B. S. and Luini, A. (2011). Models for Golgi traffic: a critical assessment. *Cold Spring Harbor Perspect. Biol.* **3**, a005215.

Grieve, A. G. and Rabouille, C. (2011). Golgi bypass: skirting around the heart of classical secretion. *Cold Spring Harbor Perspect. Biol.* **3**, a005298.

Hauri, H. P., Kappeler, F., Andersson, H. and Appenzeller, C. (2000). ERGIC-53 and traffic in the secretory pathway. *J. Cell Sci.* **113**, 587-596.

He, C. Y., Ho, H. H., Malsam, J., Chalouni, C., West, C. M., Ullu, E., Toomre, D. and Warren, G. (2004). Golgi duplication in *Trypanosoma brucei*. *J. Cell Biol.* **165**, 313-321.

Ishii, M., Suda, Y., Kurokawa, K. and Nakano, A. (2016). COPI is essential for Golgi cisternal maturation and dynamics. *J. Cell Sci.* **129**, 3251-3261.

Ito, Y., Uemura, T., Shoda, K., Fujimoto, M., Ueda, T. and Nakano, A. (2012). *cis*-Golgi proteins accumulate near the ER exit sites and act as the scaffold for Golgi regeneration after brefeldin A treatment in tobacco BY-2 cells. *Mol. Biol. Cell* **23**, 3203-3214.

Ito, Y., Uemura, T. and Nakano, A. (2014). Formation and maintenance of the Golgi apparatus in plant cells. In *International Review of Cell and Molecular Biology*, Vol. 310 (ed. W. J. Kwang), pp. 221-287. Burlington: Academic Press.

Karimi, M., Inzé, D. and Depicker, A. (2002). GATEWAY™ vectors for Agrobacterium-mediated plant transformation. *Trends Plant Sci.* **7**, 193-195.

Karimi, M., De Meyer, B. and Hilson, P. (2005). Modular cloning in plant cells. *Trends Plant Sci.* **10**, 103-105.

Kuge, O., Dascher, C., Orci, L., Rowe, T., Amherdt, M., Plutner, H., Ravazzola, M., Tanigawa, G., Rothman, J. E. and Balch, W. E. (1994). Sar1 promotes vesicle budding from the endoplasmic reticulum but not Golgi compartments. *J. Cell Biol.* **125**, 51-65.

Kurokawa, K., Ishii, M., Suda, Y., Ichihara, A. Nakano, A. (2013). Live cell visualization of Golgi membrane dynamics by super-resolution confocal live imaging microscopy. In *Methods in Cell Biology*, vol. 118 (ed. P. Franck and J. S. David), pp. 235-242. USA: Academic Press.

Kurokawa, K., Okamoto, M. and Nakano, A. (2014). Contact of cis-Golgi with ER exit sites executes cargo capture and delivery from the ER. *Nat. Commun.* **5**, 3653.

Langhans, M., Hawes, C., Hillmer, S., Hummel, E. and Robinson, D. G. (2007). Golgi regeneration after brefeldin A treatment in BY-2 cells entails stack enlargement and cisternal growth followed by division. *Plant Physiol.* **145**, 527-538.

Lippincott-Schwartz, J., Donaldson, J. G., Schweizer, A., Berger, E. G., Hauri, H.-P., Yuan, L. C. and Klausner, R. D. (1990). Microtubule-dependent retrograde transport of proteins into the ER in the presence of brefeldin A suggests an ER recycling pathway. *Cell* **60**, 821-836.

Matsuura-Tokita, K., Takeuchi, M., Ichihara, A., Mikuriya, K. and Nakano, A. (2006). Live imaging of yeast Golgi cisternal maturation. *Nature* **441**, 1007-1010.

Nagata, T., Nemoto, Y. and Hasezawa, S. (1992). Tobacco BY-2 cell line as the cell in the cell biology of higher plants. *Int. Rev. Cytol.* **132**, 1-30.

Nakano, A. and Luini, A. (2010). Passage through the Golgi. *Curr. Opin. Cell Biol.* **22**, 471-478.

Nakano, A., Otsuka, H., Yamagishi, M., Yamamoto, E., Kimura, K., Nishikawa, S.-I. and Oka, T. (1994). Mutational analysis of the Sar1 protein, a small GTPase which is essential for vesicular transport from the endoplasmic reticulum. *J. Biochem.* **116**, 243-247.

Osterrieder, A., Hummel, E., Carvalho, C. M. and Hawes, C. (2009). Golgi membrane dynamics after induction of a dominant-negative mutant Sar1 GTPase in tobacco. *J. Exp. Bot.* **61**, 405-422.

Pagny, S., Bouissonnie, F., Sarkar, M., Follet-Gueye, M. L., Driouich, A., Schachter, H., Faye, L. and Gomord, V. (2003). Structural requirements for

Arabidopsisβ1,2-xylosyltransferase activity and targeting to the Golgi. *Plant J.* **33**, 189-203.

Pelletier, L., Stern, C. A., Pypaert, M., Sheff, D., Ngô, H. M., Roper, N., He, C. Y., Hu, K., Toomre, D., Coppens, I. et al. (2002). Golgi biogenesis in *Toxoplasma gondii*. *Nature* **418**, 548-552.

Puri, S. and Linstedt, A. D. (2003). Capacity of the Golgi apparatus for biogenesis from the endoplasmic reticulum. *Mol. Biol. Cell* **14**, 5011-5018.

Rabouille, C. (2017). Pathways of unconventional protein secretion. *Trends Cell Biol.* **3**, 230-240.

Ritzenthaler, C., Nebenführ, A., Movafeghi, A., Stussi-Garaud, C., Behnia, L., Pimpl, P., Staehelin, L. A. and Robinson, D. G. (2002). Reevaluation of the effects of brefeldin A on plant cells using tobacco Bright Yellow 2 cells expressing Golgi-targeted green fluorescent protein and COPI antisera. *Plant Cell* **14**, 237-261.

Robinson, D. G., Brandizzi, F., Hawes, C. and Nakano, A. (2015). Vesicles versus tubes: is endoplasmic reticulum-Golgi transport in plants fundamentally different from other eukaryotes? *Plant Physiol.* **168**, 393-406.

Sato, K. and Nakano, A. (2007). Mechanisms of COPII vesicle formation and protein sorting. *FEBS Lett.* **581**, 2076-2082.

Schoberer, J., Runions, J., Steinkellner, H., Strasser, R., Hawes, C. and Osterrieder, A. (2010). Sequential depletion and acquisition of proteins during Golgi stack disassembly and reformation. *Traffic* **11**, 1429-1444.

Shima, D. T., Cabrera-Poch, N., Pepperkok, R. and Warren, G. (1998). An ordered inheritance strategy for the Golgi apparatus: visualization of mitotic disassembly reveals a role for the mitotic spindle. *J. Cell Biol.* **141**, 955-966.

Takeuchi, M., Tada, M., Saito, C., Yashiroda, H. and Nakano, A. (1998). Isolation of a tobacco cDNA encoding Sar1 GTPase and analysis of its dominant mutations in vesicular traffic using a yeast complementation system. *Plant Cell Physiol.* **39**, 590-599.

Takeuchi, M., Ueda, T., Sato, K., Abe, H., Nagata, T. and Nakano, A. (2000). A dominant negative mutant of Sar1 GTPase inhibits protein transport from the endoplasmic reticulum to the Golgi apparatus in tobacco and *Arabidopsis* cultured cells. *Plant J.* **23**, 517-525.

Wei, J.-H. and Seemann, J. (2010). Unraveling the Golgi Ribbon. *Traffic* **11**, 1391-1400.

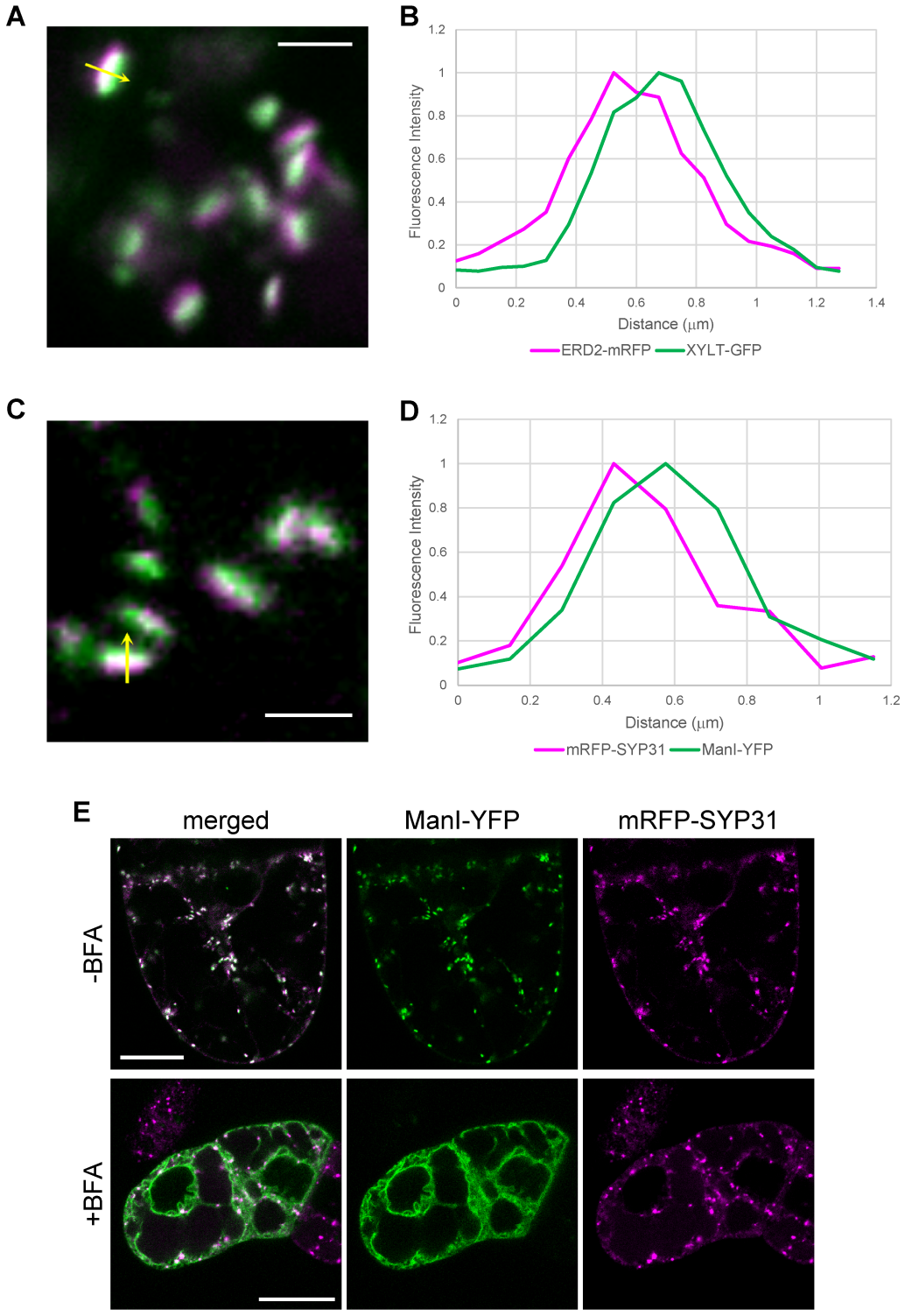

Supplementary Figure 1. Intra-Golgi localization of Golgi markers.

(A) Confocal image of BY-2 cells expressing XYLT-GFP (green) and ERD2-mRFP (magenta). The image was taken by ZEISS 780 with lambda mode, and GFP and mRFP signals were unmixed based on spectral data of the fluorescent proteins. (B) The fluorescent profile along the arrow in (A). The fluorescent intensity was normalized by the maximum value for each marker. (C) Confocal image of BY-2 cells expressing ManI-YFP (green) and mRFP-SYP31 (magenta). Observation and image processing was performed similarly to (A). (D) The fluorescent profile along the arrow in (C). The fluorescent intensity was normalized by the maximum value for each marker. (E) BFA treatment of the cells expressing ManI-YFP (green) and mRFP-SYP31 (magenta). Without BFA (-BFA) and with 1.5 h of 50 μM BFA treatment (+BFA). Representative images from at least 5 independent cells for each condition. Scale bars, 2 μm (A, C) and 20 μm (E).

Journal of Cell Science • Supplementary information

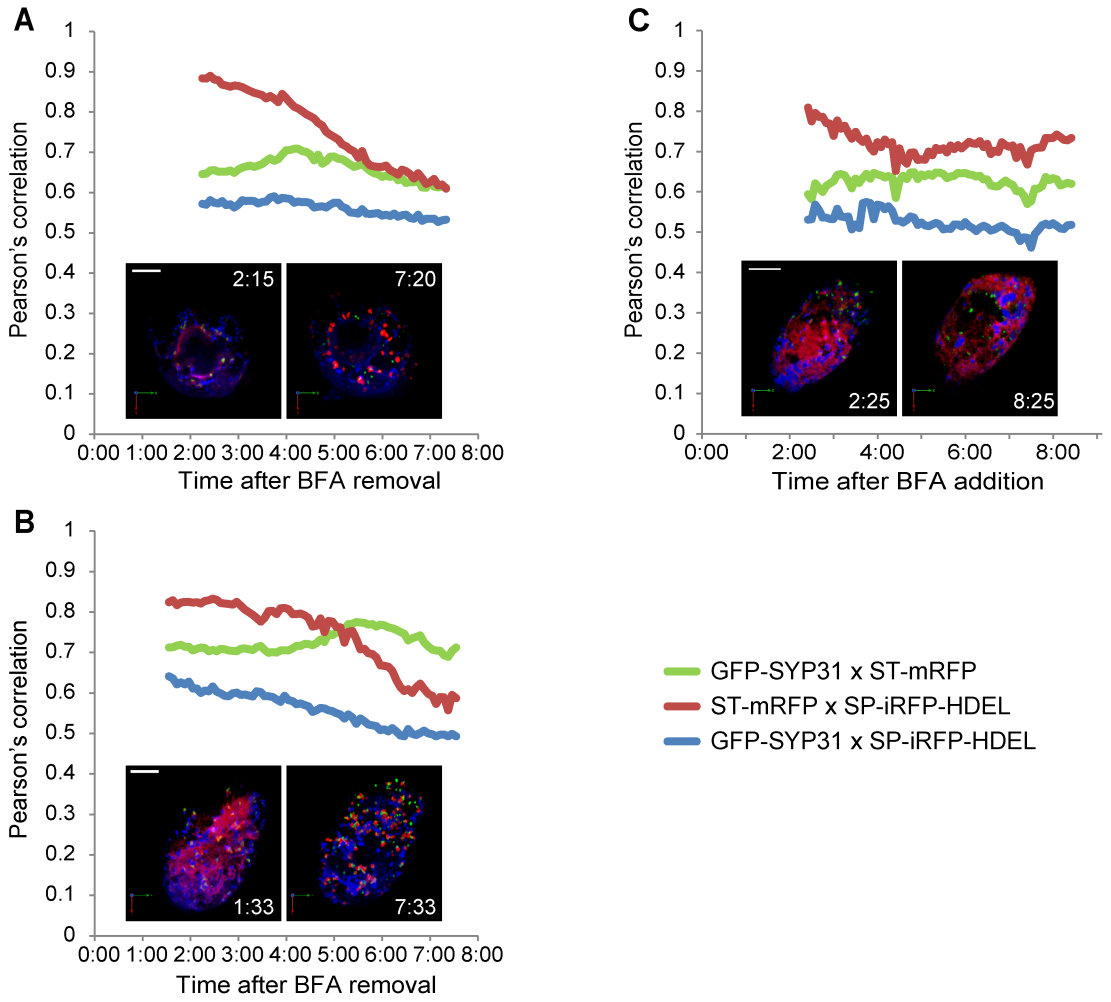

Supplementary Figure 2. 3D Pearson's correlation coefficients of Golgi and ER markers during Golgi regeneration.

Time-lapse 3D observations were performed on BY-2 cells expressing GFP-SYP31 (*cis*, green), ST-mRFP (*trans*, red), and SP-iRFP-HDEL (ER, blue) by SCLIM with 5 min intervals, and the change of 3D Pearson's correlation coefficients over time are presented in graphs. (A, B) The cells with BFA treatment followed by its removal. The cells were treated by drugs in the same procedure that was taken for the cells in Figure 3A. The indicated times mean the elapsed time after BFA removal. (C) The cells treated with BFA without removal. The cells were treated with BFA and biliverdin in advance, LatB was added 1.5 h after BFA addition, and cycloheximide was added 30 min after LatB addition. Indicated times mean the elapsed time after BFA addition. Scale bars, 10 µm.

Journal of Cell Science • Supplementary information

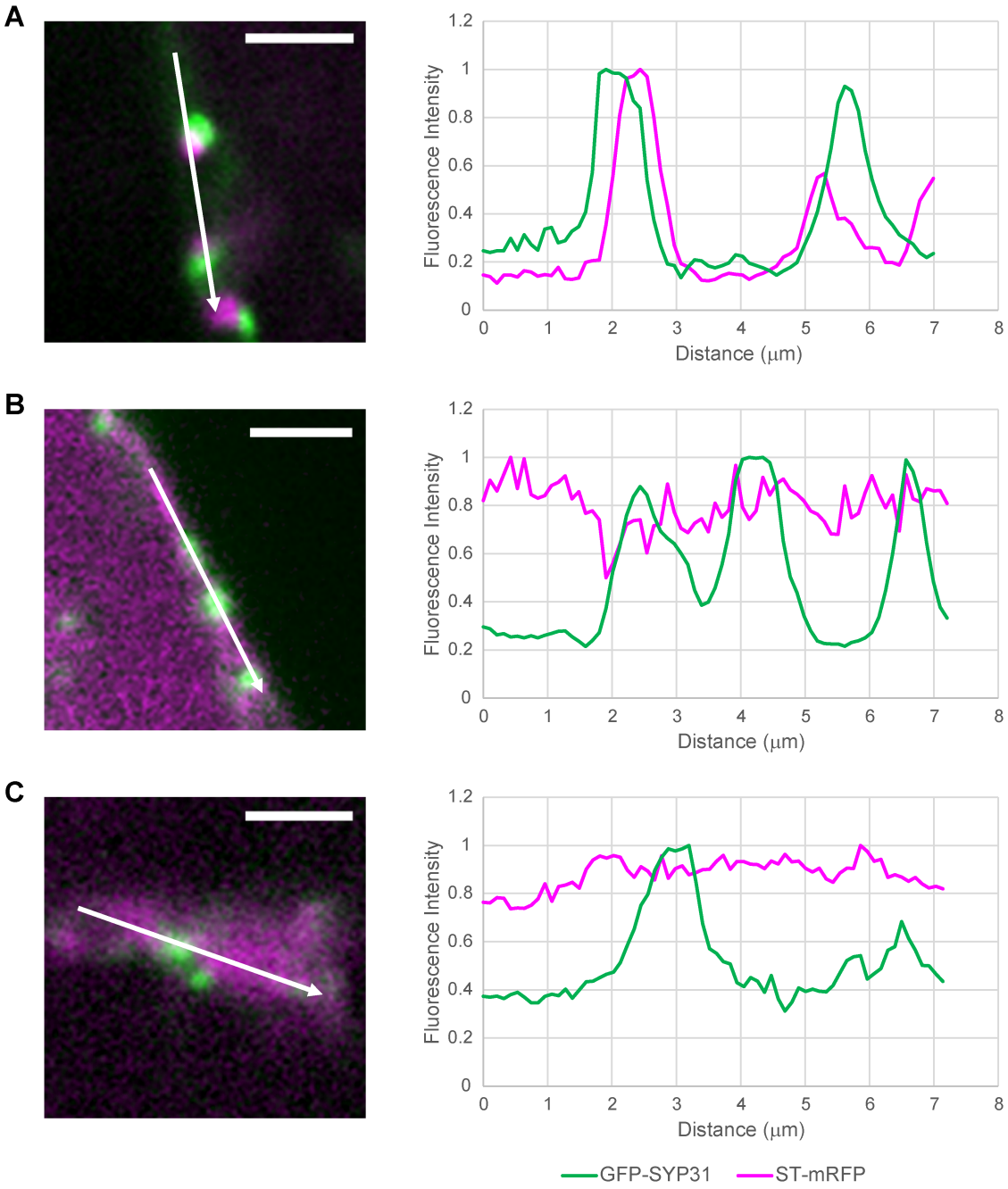

Supplementary Figure 3. Fluorescent profile around GECCO upon induction of NtSAR1 H74L. Confocal images of BY-2 cells expressing GFP-SYP31 (green) and ST-mRFP (magenta) with or without NtSAR1 H74L induction (left), and the fluorescent profile along the arrows (right). The fluorescent intensity was normalized by the maximum value for each marker in each graph. (A) The cell shown in Figure 5A (-DEX). GFP-SYP31 and ST-mRFP were stably expressed without NtSAR1 H74L induction. (B) The cell shown in Figure 5A (+DEX). GFP-SYP31 and ST-mRFP were stably expressed, and NtSAR1 H74L was induced. (C) The cell shown in Figure 5C. GFP-SYP31 and ST-mRFP were induced after induction of NtSAR1 H74L. Scale bars, 3 μm.

Journal of Cell Science • Supplementary information